The Korean Journal of Ceramice, 5[3] 270-277 (1999)

Ballistic Resistance of an Armor Ceramic Structure against a Shaped Charge Jet As a Function of Penetration Depth

Hyunho Shin, Chang-Hyun Lee, and Wan Sung

Agency for Defense Development, 1'st R & D Center
P.O. Box 35-1, Yousung, Taejon, Rep. of KOREA
(Received September 23, 1998)

The ballistic capability of an alumina-rich oxide armor ceramic against a shaped charge jet was characterized as a function of penetration depth in a layered target structure. The penetration resistance of the ceramic, based upon the determination of penetration velocity, was not equally realized throughout the depth of penetration. It was abnormally low at an early stage of penetration, followed by a sudden increase to reach ~16GPa thereafter. There was no apparent change in such a profile with respect to the lateral size of the specimen. Based upon 2-D flash x-ray radiography and 3-D Hull code simulation, the feasibility of forming a pressure-induced predamaged zone in front of the jet tip was speculated to foster an increased penetration velocity in the initial stage penetration, resulting in the diminished penetration resistance. The disappearance of such a predamaged zone with penetration was interpreted to restore the resistance of the ceramic in the later penetration stage.

Key words: Armor ceramic, Penetration resistance, Ballistic efficiency, Shaped charge

I. Introduction

In general, structural ceramic materials for armor applications (Al_2O_3, SiC, TiB_2, B_4C, etc.)[1,2] show higher ballistic efficiencies against a hyper velocity projectile (shaped charge jet) as compared to the low speed (<2 km/sec) kinetic projectiles (long-rod penetrator). The empirical penetration resistance, σ, of ceramics against a low velocity kinetic projectile has been 5 ~ 10 GPa,[3,4] which is around Hugoniot elastic limit (HEL: elastic limit stress required for a plastic deformation under an action of dynamic uniaxial strain). The penetration resistance against a higher speed shaped charge jet for many structural ceramics were 20 ~ 30 GPa,[5] which is 3 ~ 4 times higher than the HEL for alumina. On the other hand, the penetration resistance of metallic targets reaches 3 ~ 4 times the HEL even against the low speed kinetic projectiles.[6] That means ceramics show a low σ/HEL ratio for a low speed projectile and hence the ballistic capability of ceramics is not fully realized against such a projectile.

For the interpretation of such a phenomenon, Sternberg[7] related it to the different fracture toughness properties of ceramics and metals. When a low speed projectile is penetrating, a shock wave-induced crack would propagate ahead of projectile, resulting in a relatively low σ/HEL ratio. Then as Hauver *et al.*[8] claimed, when the penetration velocity is sufficiently high, cracks would not be able to propagate ahead of the penetrator, permitting the realization of high penetration resistance of a ceramic. Other proposed mechanisms of high ballistic efficiency of ceramics against a shaped charge jet include lateral disturbance of jet[9,10] since the jet has a higher length to diameter ratio than the long-rod penetrator.

The ballistic performance of the ceramic against a long-rod penetrator has been shown to be realized differently depending upon penetration depth and test conditions.[8] In the present study, the profile of the penetration resistance of a layerd ceramic (alumina-rich) structure against a shaped charge jet was uncovered as a function of penetration depth. This was to evaluate whether the high ballistic capability of the ceramic is demonstrated equally throughout the penetration depth or not.

II. Penetration by a Hyper Velocity Projectile

1. Shaped Charge Jet

The shaped charge is composed of a cylindrical container, which has one side with flat ended surface and other side with a conical metallic liner as shown in Fig. 1. It contains

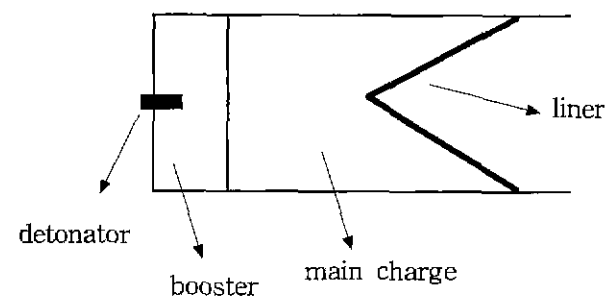

Fig. 1. Schematic diagram of shaped charge.

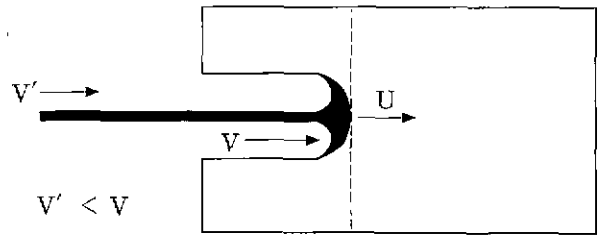

Fig. 2. Schematic of jet penetration into a target.

main charge and booster inside and detonator, to trigger the explosion process, positioned at the flat ended side. When the main charge is exploded, the conical metallic liner is deformed to form a elongated structure (Fig. 2) which serves as a penetrator.[11] The high-strain and high-strain-rate state of the liner material formed via a shaped charge explosion is called "jet" and its physical nature has been under active studies. It has a granular microstructure, presumably via a dynamic recovery process,[12] while it was thought a melted state initially. In general, the jet has an approximately linear velocity gradient (flying velocity decreases from tip to the tail) so that the length of the jet extends as time passes and finally breaks up to many particulates. The tip velocity is of the order of several km/sec.

2. Penetration Resistance and Ballistic Efficiency

The pressure induced by the collision of a hypervelocity projectile to a target material reaches several giga pascals (much higher than target yield strength), leading one to describe the penetration phenomena hydrodynamically. Then the pressure at both sides of the penetrator/target interface shown in Fig. 2 is equal.[11] Recalling Bernoulli's principle,

$$P = \frac{1}{2}\rho_p(V-U)^2 = \frac{1}{2}\rho_t U^2 \tag{1}$$

where P is the pressure at penetrator/target interface, V the velocity of jet component at interface, U the penetration (or interface) velocity, ρ the density, and the subscripts p and t represent jet penetrator and target, respectively. When reading Lagrangian coordinate at the interface, $|V-U|$ is the incoming particle velocity from the jet to the interface and $|U|$ is the incoming particle velocity from the target to the interface. In order to account for the difference between the results from eq. (1) and many empirical results, eq. (1) has been modified[13]:

$$\frac{1}{2}\rho_p(V-U)^2 + Y_p = \frac{1}{2}\rho_t U^2 + R_t$$

$$\rho_p(V-U)^2 = \rho_t U^2 + 2\sigma \tag{2}$$

where Y_p and R_t is the pressure term associated with the projectile and target material, respectively. Sigma corresponds to R_t-Y_p. In general, for copper jet and many high-hardness armor ceramic targets, Y_p is negligible as compared to R_t, implying $\sigma \approx R_t$.

An efficient armor ceramic would show a diminished ratio of penetration velocity U to the jet velocity V. A high value of sigma indicates a diminished U/V ratio as seen in eq. (3), derived from eq. (2) for continuous jet (gamma=1),

$$\frac{V}{U} = 1 + \sqrt{\frac{\rho_t}{\gamma\rho_p} + \frac{2\sigma}{\gamma\rho_p U^2}} \tag{3}$$

where, gamma is the correction factor for the degree of jet break up ($0<\gamma\leq 1$). Thus sigma is named "penetration resistance" representing the capability of an armor material. The capability of an armor ceramic can also be evaluated by the test methodology shown in Fig. 3, which results in the concept of "ballistic efficiency", ε.[14]

$$\varepsilon = \frac{\rho_o(P_o - P)}{\rho_c T} \tag{4}$$

where ρ_0 and ρ_c are density of metallic reference and armor ceramic, respectively, T is the thickness of armor ceramic, P_0 is the penetration depth in the reference when no armor ceramic is used, and P is the residual depth of penetration in the reference when an armor ceramic is applied. An armor ceramic with ballistic efficiency of epsilon requires $1/\varepsilon$ times the mass of reference material in order to defeat a given threat.

In general, an armor material with high penetration resistance, determined by the measurement of penetration

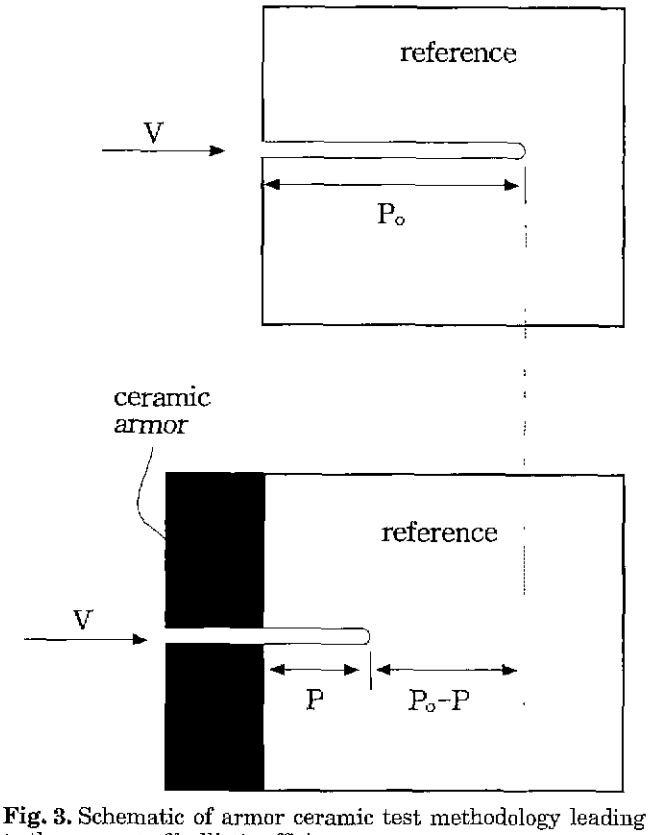

Fig. 3. Schematic of armor ceramic test methodology leading to the concept of ballistic efficiency.

velocity, results in a high ballistic efficiency, while it is not always the case especially when lateral disturbance of jet is significant.[15]

III. Experimental Procedure

1. Measurement of Penetration Time

The shaped charge used in this study had Comp. B as main charge and a copper cone liner with outer charge diameter of 40 mm. The velocity of the jet tip was 6.63 km/sec. The schematic diagram for the experimental condition is shown in Fig. 4. The target is composed of three layers of ceramic tiles (100×100×25 mm) followed by several layers of mild steel witness plates (100×100×22 mm). The ceramic material had an alumina-rich composition with apparent density of 2.7 g/cm^3. The distance from the cone base to the surface of the ceramic target structure (stand off) was 3.5 times the charge diameter. In order to count the required time for the arrival of jet to penetration steps available in the target structure, four sets of make-screens were placed in the target as shown in Fig. 4. Each set of make-screen was composed of two 0.5 mm thick aluminum sheets with a 0.2 mm thick insulating film between them. The aluminum sheets were then electrically connected to a circuit (event detector) generating an electrical signal when the penetrating copper jet mechanoelectrically connects aluminum sheets of each make-screen. The signal from the circuit was monitored via an oscilloscope.

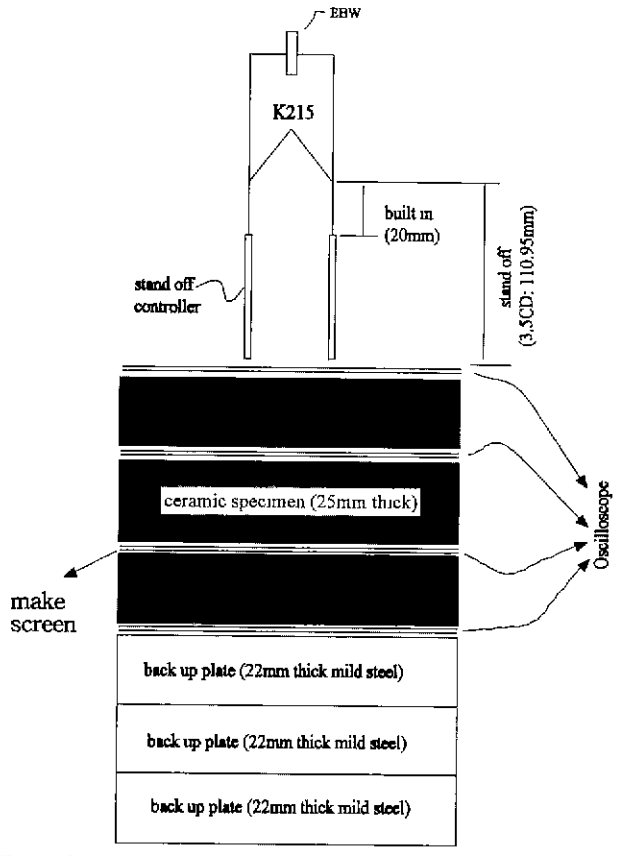

Fig. 4. Schematic of experimental set up.

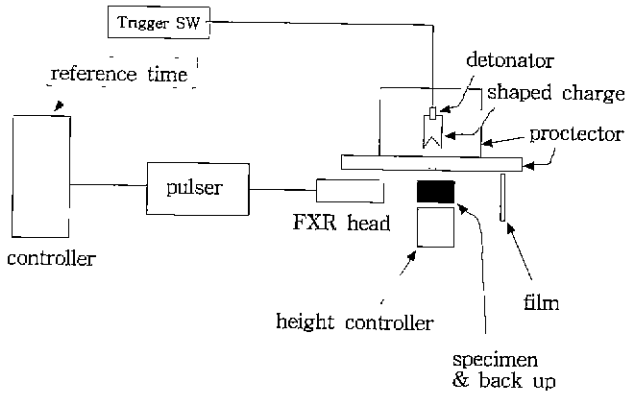

Fig. 5. Schematic of flash X-ray radiography.

2. Flash X-ray Radiography

The flash X-ray radiography (FXR) used in ballistics area differs from the X-ray diffractometry (XRD) in materials analysis in that FXR utilizes penetration capability of X-ray with various wavelengths while XRD employs the diffracting nature of a monochromatic X-ray. FXR requires a much higher power (0.1 to few mega volts) for short duration of time (~nano seconds) in order to capture the pene-

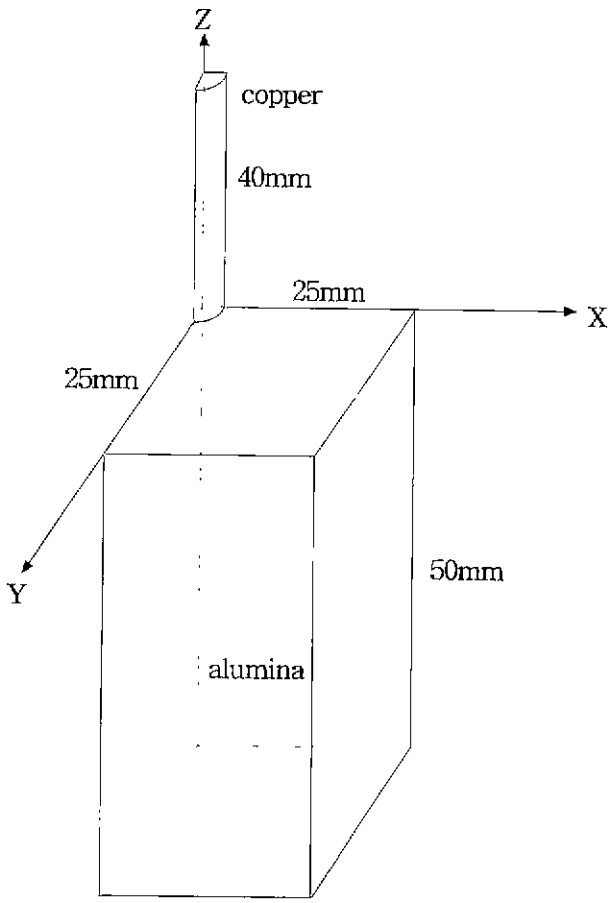

Fig. 6. Geometry for Hull code simulation.

tration event by a hyper velocity projectile. Fig. 5 shows schematic diagram for capturing the jet penetration phenomena into the ceramic structure. For the FXR radiography in this work, the size of the ceramic specimen at each layer was 50×50×25(mm) considering the penetrating capability of the utilized FXR system.

3. Hull Code Simulation

In order to uncover the characteristics of early stage penetration, the penetration phenomenon was simulated using a hydrodynamic code Hull (Orlando Technology, Incorporated, Shalima, FL, U.S.A.). This program is based on the finite differential method and can employ either Eulerian or Lagrangian coordinate system. The simulation situation was the collision of cylinder type copper rod (Φ3×40 mm) in Eulerian coordinate with velocity of 6km/sec into an alumina ceramic with density of 3.9 g/cm^3. Considering the symmetry of the simulating structure, 1/4 of the geometry was calculated as shown in Fig. 6.

IV. Results and Discussion

1. Penetration Resistance As a Function of Penetration Depth

Fig. 7 shows the measured penetration time at penetration depth of 25, 50, and 75 mm. These depths represent the boundary between the target layers. From these data, the average penetration velocity of the jet at each ceramic layer was obtained and are shown in Fig. 8. Fig. 9 shows the penetration event captured by FXR radiography. From Fig. 9, the penetration into the studied armor ceramic is believed to be completed by a continuous jet.

From Figs. 7-8, the lateral size of the ceramic specimen shows no distinct effect on the average penetration velocity at each layer. Thus all the data in Fig. 7 were combined to

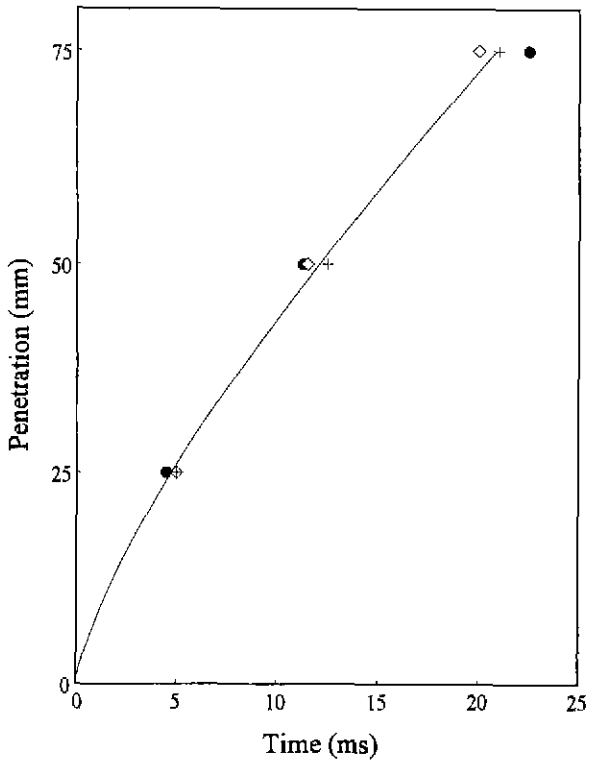

Fig. 7. Change in penetration depth as a function of penetration time for specimens with lateral sizes of 100 cm^2(◇, +) and 25 cm^2(●).

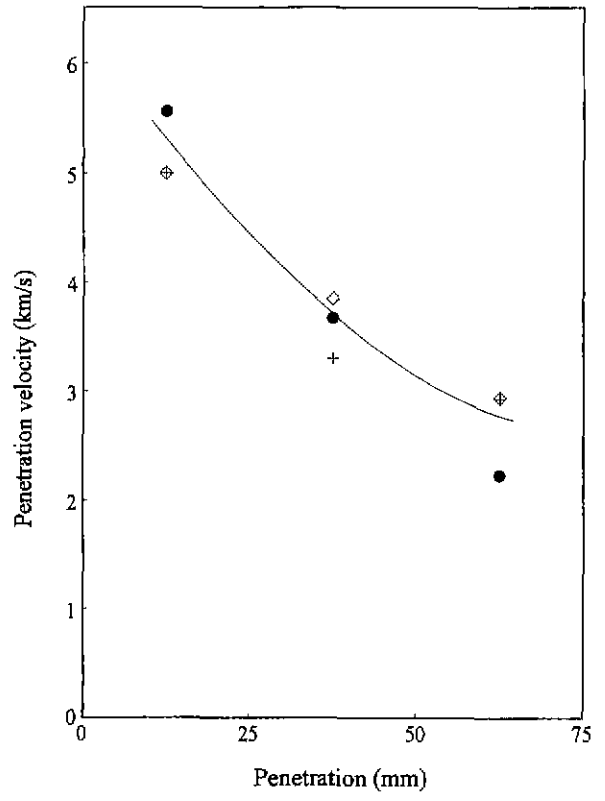

Fig. 8. Change in average penetration velocity at midpoint of each layer for specimens with lateral sizes of 100 cm^2(◇, +) and 25 cm^2(●).

Fig. 9. 2-D flash radiography for jet penetration into the ceramic layers at 33 ms after jet collision on the target surface (each layer with 50×50×25 μm-sized specimen).

result in a regression relation between penetration depth and penetration time:

$$P=7.8631\ t^{0.7422} \quad (5)$$

where, P is the penetration depth (mm) and t is the penetration time (μs) counted from the collision of the jet to the surface of the first ceramic layer. The solid line in Fig. 7 is based upon equation (5).

By differentiating equation (5) with respect to penetration time and expressing in terms of penetration depth, the relation between penetration velocity U and penetration depth P is obtained as:

$$U=11.9453\ P^{0.3473} \quad (6)$$

The change in penetration velocity, U, as a function of penetration depth based upon equation (6) is shown in Fig. 10. The velocity of arriving jet to the jet/target interface, V, is also shown in Fig. 10. This was obtained by considering flying distance and flying time of the jet from the virtual origin (point where all jet components form).

$$V = \frac{S_0 + P}{t_0 + t} \quad (7)$$

where S_o is the distance from virtual origin to the surface of the first ceramic layer, t_o is the required time for the jet segment of V to travel S_o, P is the penetration depth counted from the surface of the first ceramic layer, and t is the required time for the jet to penetrate the depth of P in the ceramic.

Based upon the assumption of hydrodynamic penetration (σ=0), the reference U/V value from equation (3) is 0.645. The hydrodynamic limit for the penetration velocity U_{hyd} shown in Fig. 10 was obtained by multiplying 0.645 to the jet velocity V. As shown in the figure, the penetration velocity U is greater than the hydrodynamic limiting velocity U_{hyd} until the penetration depth of 21 mm (roughly in the first ceramic layer), while the trend is reversed thereafter. In Fig. 10, penetration velocity U, the result of the differentiation of P-t curve in Fig. 7, appears abnormally high in early stage of penetration. Since the P-t data in that region (up to 21 mm penetration depth) is an approximation, the absolute value of U at each penetration depth (Fig. 10) is hard to assign much physical significance. However, the required time to reach 25 mm depth of penetration is certainly faster (Fig. 7) than the hydrodynamically predicted time, resulting in a fairly high average U in this region (Fig. 8). Thus the fact itself that $U>U_{hyd}$ in this region is apparent.

Fig. 11 shows the change in U/V as a function of penetration depth (dotted curve). Shown in Fig. 11 is also the resultant penetration resistance σ (solid curve) determined by equation (3). As shown in the figure, penetration resistance of the ceramic is negative until penetration depth of ~21 mm followed by a sudden increase to reach 16 GPa thereafter.This result indicates that the ballistic performance of the studied ceramic structure is not equally real-

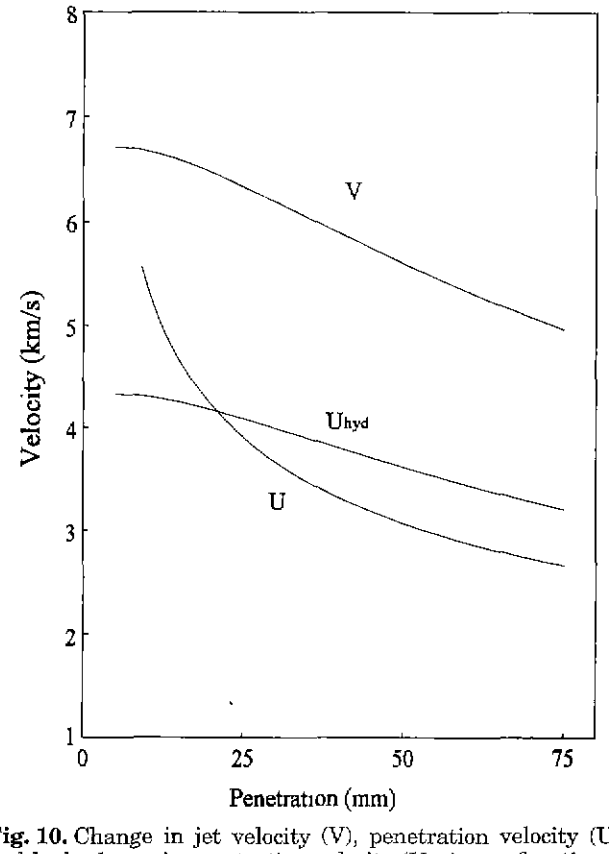

Fig. 10. Change in jet velocity (V), penetration velocity (U), and hydrodynamic penetration velocity (U_{hyd}) as a function of penetration depth.

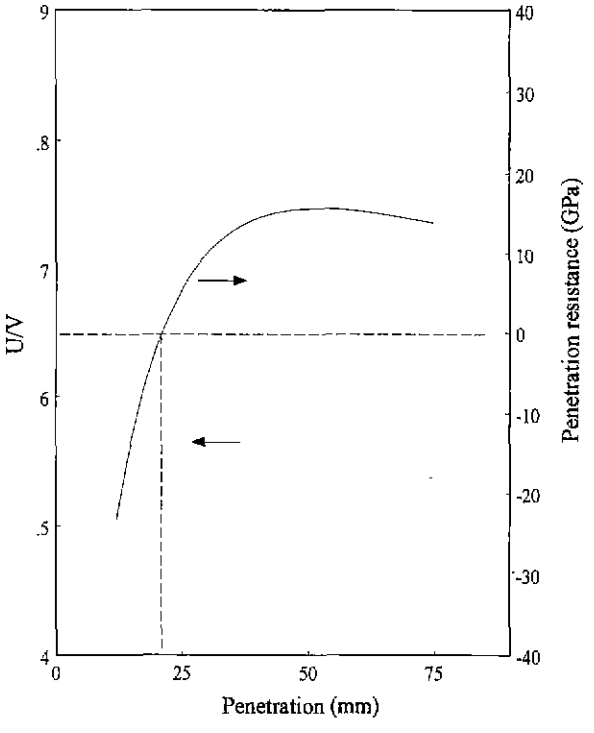

Fig. 11. Change in U/V and penetration resistance as a function of penetration depth

ized throughout the penetration depth. The maximal penetration resistance of the studied ceramic structure against a shaped charge jet (16 GPa) is lower than that of high hardness ceramics[9] such as B_4C (33 GPa) and SiC (25 GPa), while similar to that of relatively soft SiO_2 based oxide ceramic (15 GPa).

As illustrated in Fig. 11, U/V less than 0.645 results in the positive penetration resistance and vice versa for the case of U/V higher than the reference value. The lower U and U/V than the reference value roughly in the second and third ceramic layer are certainly due to the realization of the ballistic resistance of the ceramic material.

The negative value of the penetration resistance in the first layer (Fig. 11) is physically due to higher penetration velocity($U>U_{hyd}$ until penetration depth of ~21 mm in Fig. 10). This means that, in the first layer, the penetration resistance of the armor ceramic is inferior to the ballistic resistance of a fluid with the same density as the ceramic. Such a behavior is consistent with the inferior *ballistic efficiency* of the ceramic in the first layer, as determined by the measurement of residual depth of penetration (equation 4) in separate works. For a number of ceramics, the ballistic efficiency of the ceramic at the first layer (against a shaped charge) is inferior to the values obtained when the ceramic is positioned in the second or third layer. In extreme cases, the ballistic efficiency in the first layer showed up to be negative, as if the ceramic were behaving to assist jet penetration. All these behaviors would be associated with the abnormally high penetration velocity in the first layer.

2. Penetration Resistance in the Initial Stage of Penetration

2-1. Cratering Effect

For a plausible interpretation for the high penetration velocity in the first layer, first, notice the large penetration crater near the top surface (until penetration depth of 8.1 mm) in Fig. 11, followed by a steady and relatively narrow penetration crater. At first glance, the large penetration crater in the first ceramic layer seems to be associated with high penetration velocity (high U/V) in that area. The large penetration crater would be the result of at least two qualitative reasons: either a free surface effect due to the asymmetric bonding of the material in the surface or the effect of transverse component of Rayleigh wave.[16] The transverse component of Rayleigh wave decays exponentially with penetration depth. An in-depth correlation of the large crater size to the high U requires further study. Since the large crater zone (~8.1 mm) cannot fully cover the high penetration speed zone (~21 mm of the penetration depth), other reasons for the high penetration speed in the first layer should also be pursued.

2-2. Peak Pressure Effect

It is informative to recall the work of Christman and Gehring[17] who pointed out that there was an initial peak pressure zone at a penetrator/target interface. A qualitative diagram by them is shown in Fig. 12. In this figure, the

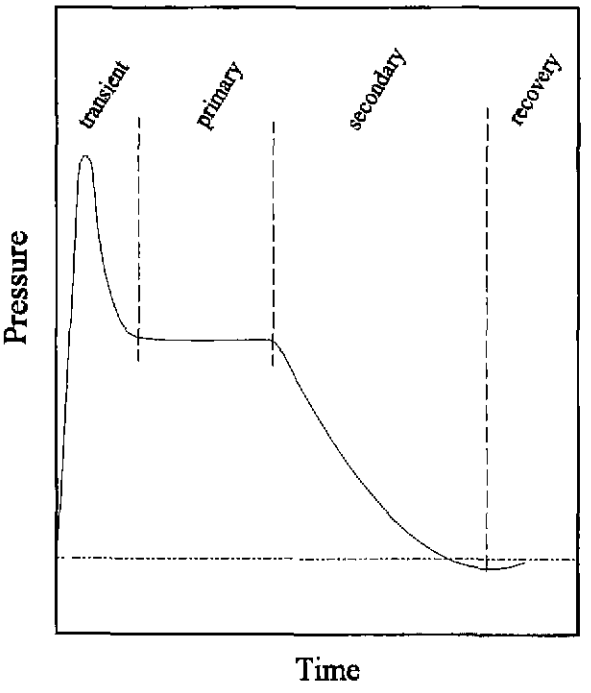

Fig. 12. Qualitative diagram for the pressure at penetrator/target interface during penetration.[17]

transient zone, which lasts several microseconds, is of our concern. The issue is that how much the transient pressure rises and how it attenuates with penetration depth in the studied system, since such an information would provide a clue for the initial penetration behavior.

In order to obtain the pressure build-up, the velocity of shock wave, U_s, ahead of the penetrator, should be known. For a transparent target material, this can be monitored using a high speed camera. Then the pressure, P, in the shocked region can be obtained using the equation of state,[18]

$$U_s = C_0 + S_1 U_p + S_2 U_p^2 + \cdots \quad (8)$$

$$P = \rho_0 U_s U_p \quad (9)$$

where ρ_0 is the density of target material, U_p is the velocity of particle, and C_0, S_1, and S_2 are the constants correlating U_s and U_p. Data base for these constants for many materials are available.[19]

For non-transparent materials like the specimen studied in this work, however, the determination of shock wave velocity especially during penetration is difficult. Thus, a computer simulation using HULL code was adopted in this work for the illustration of pressure profile with penetration depth. Since many dynamic material properties are not yet established for the studied alumina-based armor ceramic, simulation of copper jet penetration was performed for pure Al_2O_3 target. Fig. 13 shows the simulated XZ plane of the 3-D structure for the penetration event at 7 μs after the collision. As shown in the figure, the pressure build-up ahead of the penetrator[20] is apparent.

The pressure rise at finite number of positions in Z axis

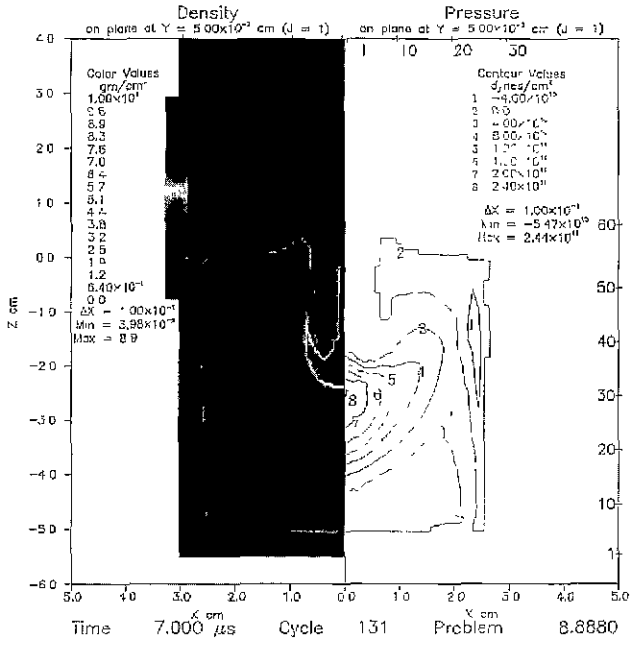

Fig. 13. Simulation result for the penetration of copper rod into alumina at 6 km/sec (after 6 μs after collision).

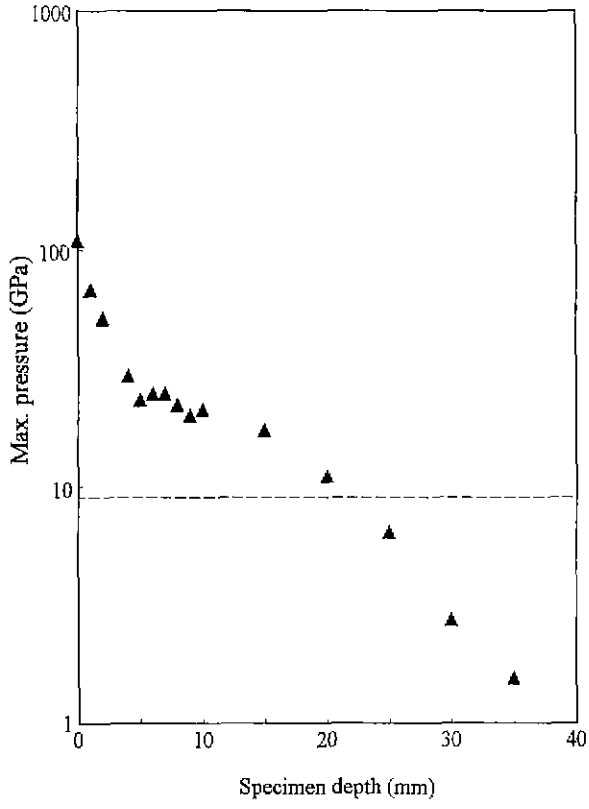

Fig. 14. Simulated maximun pressure built-up in alumina specimen as a function of specimen depth by the penetration of copper rod at 6 km/sec.

were monitored as a function of penetration time and the maximum peak pressure at each position is illustrated in Fig. 14. As shown in the figure, the peak pressure at the initial collision surface reaches as high as 110 GPa followed by a sharp decay as penetration proceeds. A calculation based upon the impedance matching technique[18] for copper plate impact to an alumina plate using eqs. 8-9 resulted in even higher value of 160 GPa at the surface. After the penetration depth of 5 mm, the rate of decay is attenuated followed by an increase in decay rate after 20 mm penetration depth. After 20~25 mm penetration depth range, the pressure build-up is lower than the dynamic compressive strength[21] of the target material. Considering the decreasing jet velocity profile from jet tip, such a transition point for a real jet would be located at a smaller depth into alumina.

The extremely higher pressure as compared to the dynamic compressive strength of the ceramic, induced in the initial stage of penetration, implies the feasibility of forming a predamage in the path of penetration. In case the form of a predamage in the ceramic is a pulverization with micropores, such a zone would allow a higher penetration velocity of jet compared to the virgin material with original density, ρ_0, implying an inferior penetration resistance sigma. Such a pulverized zone is not the result of the propagation of the slow (<2.2 km/sec for BK-7 glass[22]) cracks. Since cracks may not propagate ahead of the faster jet as many researchers asserted,[7,8] this work shows the feasibility of forming a predamaged area by a different mechanism, i.e., the build-up of pressure.

V. Conclusion

The ballistic capability of the alumina-rich oxide ceramic structure against a shaped charge jet was not equally realized throughout the depth of the structure. The penetration resistance of the ceramic structure was abnormally low up to ~21 mm penetration depth while the penetration resistance was realized thereafter to reach 16 GPa. There was no apparent change in such a profile with respect to the lateral size of the structure. Based upon 2-D flash X-ray radiography and 3-D Hull code simulation, the enlarged penetration hall and peak pressure-induced predamaged zone (associated with a large crater) were speculated to foster an increased penetration speed at the initial stage, resulting in the low penetration resistance. The decay of such a pressure build-up with penetration depth was interpreted to restore the high ballistic capability of the ceramic in the second and third ceramic layers.

References

1. S. K. Chung, "Fracture Characterization of Armor Ceramics," *Am. Ceram. Soc. Bull.*, **69**(3), 358-366 (1990).
2. D. J. Viechnicki, M. J. Slavin, and M. I. Kliman, "Development and Current Status of Armor Ceramics," *Am. Ceram. Soc. Bull.*, **70**(6), 1035-1039 (1991).
3. Z. Rosenberg and J. Tsaliah, "Applying Tate Model for the Interaction of Long Rod Projectiles with Ceramic Targets," *Int'l. J. Impact Eng.*, **9**, 247-256 (1990).
4. S. J. Bless and C. E. Anderson, Jr., "Penetration of Hard

Layers by Hypervelocity Rod Projectiles," *Int'l. J. Impact. Engng.*, **14**, 85-93 (1993).
5. A. A. Kozhushko, I. I. Rykova and A. B. Sinani, "Resistance of Ceramics to Penetration at Impact Velocities above 5 km/sec," *J. de Physique (Colloq., C3, Suppl. III)*, **1**, C3-117 (1992).
6. A. Tate, "A Theory for the Deceleration of Long Rods After Impacts," *J. Mech. Phys. Solids*, **15**, 387-399 (1967).
7. J. Sternberg, "Material Properties Determining the Resistance of Ceramics to High Velocity Penetration," *J. Appl. Phys.*, **65**, 3417-3424 (1989).
8. G. E. Hauver, P. H. Netherwood, R. F. Bench, W. A. Gooch, W. J. Perciballi and M. S. Burkins, "Variation of Target Resistance during Long-Rod Penetration into Ceramic"; pp. 257-264 in Proceedings of 13th Int'l. Symp. on Ballistics, American Defense Preparedness Association, 1992.
9. A. A. Kozhushko, I. I. Rykova and A. B. Sinani, "Resistance of Ceramics to Projectile Penetration at High Interaction Velocities," *Combustion Explosives and Shock Waves*, **28**, 84-88 (1992).
10. G. Solve and J. Cagnoux, "The Behavior of Pyrex Glass Against a Shaped-Charge Jet"; pp. 967-970 in *Shock Compression of Condensed Matter-1989*, Edited by, S. C., Schmidt, J. N., Johnson, and L. W. Davison, Elsevier Science Pub., New York, 1990.
11. G. Birkhoff, D. P. MacDougall, E. M. Pugh and S. G. Taylor, "Explosives with Lined Cavities," *J. Appl. Phys.*, **19**, 563- 582 (1948).
12. M. A. Meyers, L. W. Meyer, J. Beatty, U. Andrade, K. S. Vecchio and A. H. Chokshi, "High Strain, High-Strain-Rate Deformation of Copper," in *Shock Wave and High-Strain-Rate Phenomena in Materials*, pp. 529-542, Eds., M. A. Meyers, L. E. Murr, and K. P. Staudhammer, Marcel Dekker, Inc., New York (1992).
13. R. J. Eichelberger, "Experimental Test of the Theory of Penetration by Metallic Jets," *J. Appl. Phys.*, **27**(1), 63-68 (1956).
14. D. Yaziv, G. Rosenberg and Y. Partom, "Differential Ballistic Efficiency of Applique Armor"; pp. 315-319 in Proceedings of 9th Int'l. Symp. on Ballistics, Vol. 2, American Defense Preparedness Association (1986).
15. H. Shin and C. H. Lee, "An Analysis of Ballistic Properties of a Ceramic Material against a Shaped Charge Jet," *J. Defense Technical Res.*, **4**(3), 141-150 (1998).
16. H. Kolsky, *Stress Waves in Solids*, Dover, New York (1963).
17. D. R. Christman and J. W. Gehring, "Analysis of High-Velocity Projectile Penetration Mechanics," *J. Appl. Phys.*, **37**(4), 1579-1587 (1966)
18. M. A. Meyers, *Dynamic Behavior of Materials*, John Wiley & Sons, Inc., New York (1994).
19. S. P. Marsh, *LASL Shock Hugoniot Data*, University of California Press, Berkeley, CA (1980).
20. J. F. Mescall and C. Tracy, "Improved Modelling of Fracture in Ceramic Armors"; pp. 41-51 in Proceedings of 1986 Army Sci. Conf., Vol. 3, West Point, New York (1986).
21. Z. Rosenberg and Y. Yeshurun, "The Relation Between Ballistic Efficiency and Compressive Strength of Ceramic Tiles," *Int'l J. Impact Eng.*, **7**(3), 357-362 (1988).
22. J. H. Choi, C. H. Lee, S. N. Chang and S. K. Moon, "Long-Rod Impact Phenomena: Role of Wave Interaction on Crack Propagation," *Int'l J. Impact Engng.*, **17**(1-6), 195-204 (1995).